Pattern Recognition Receptor MDA5 Modulates CD8+ T Cell-Dependent Clearance of West Nile Virus from the Central Nervous System

Helen M. Lazear,[a] Amelia K. Pinto,[a] Hilario J. Ramos,[d] Sarah C. Vick,[a] Bimmi Shrestha,[a] Mehul S. Suthar,[e] Michael Gale, Jr.,[d] Michael S. Diamond[a,b,c]

Departments of Medicine,[a] Pathology & Immunology,[b] and Molecular Microbiology,[c] Washington University School of Medicine, St. Louis, Missouri, USA; Department of Immunology, University of Washington School of Medicine, Seattle, Washington, USA[d]; Department of Pediatrics, Emory Vaccine Center, Emory University, Atlanta, Georgia, USA[e]

Many viruses induce type I interferon responses by activating cytoplasmic RNA sensors, including the RIG-I-like receptors (RLRs). Although two members of the RLR family, RIG-I and MDA5, have been implicated in host control of virus infection, the relative role of each RLR in restricting pathogenesis *in vivo* remains unclear. Recent studies have demonstrated that MAVS, the adaptor central to RLR signaling, is required to trigger innate immune defenses and program adaptive immune responses, which together restrict West Nile virus (WNV) infection *in vivo*. In this study, we examined the specific contribution of MDA5 in controlling WNV in animals. $MDA5^{-/-}$ mice exhibited enhanced susceptibility, as characterized by reduced survival and elevated viral burden in the central nervous system (CNS) at late times after infection, even though small effects on systemic type I interferon response or viral replication were observed in peripheral tissues. Intracranial inoculation studies and infection experiments with primary neurons *ex vivo* revealed that an absence of MDA5 did not impact viral infection in neurons directly. Rather, subtle defects were observed in CNS-specific CD8+ T cells in $MDA5^{-/-}$ mice. Adoptive transfer into recipient $MDA5^{+/+}$ mice established that a non-cell-autonomous deficiency of MDA5 was associated with functional defects in CD8+ T cells, which resulted in a failure to clear WNV efficiently from CNS tissues. Our studies suggest that MDA5 in the immune priming environment shapes optimal CD8+ T cell activation and subsequent clearance of WNV from the CNS.

Vertebrate cells use a variety of proteins to detect viral infection. These sensors recognize non-self molecular signatures, chiefly foreign nucleic acid motifs, termed pathogen-associated molecular patterns (PAMPs). PAMPs are detected by cellular pattern recognition receptors (PRRs), which initiate signal transduction cascades that activate the host antiviral response. Two key classes of PRRs against RNA viruses include the Toll-like receptor (TLR) family, whose members detect extracellular and endosomal PAMPs, and the RIG-I-like receptor (RLR) family, which detects PAMPs in the cytoplasm (1–4). The RLR family includes three members: RIG-I, MDA5, and LGP2, encoded by the genes *Ddx58*, *Ifih1*, and *Dhx58*, respectively. RIG-I and MDA5 have similar domain organizations consisting of two tandem N-terminal caspase recruitment domains (CARDs), a central DexD/H box helicase domain with ATPase activity, and a C-terminal repressor domain (5, 6). LGP2 is distinct from the other RLRs in that it possesses helicase and regulatory domains but lacks CARDs, and it is thus believed to serve as a regulator of RLR signaling (7–10). RIG-I and MDA5 recognize distinct RNA ligands, with RIG-I preferentially recognizing 5′ triphosphate (5′-ppp) RNA encoding a short double-stranded RNA (dsRNA) motif or a single-stranded polyuridine or polycytosine motif, and MDA5 recognizing longer dsRNA motifs (11–18). Upon RNA binding to the repressor domain, RIG-I and MDA5 undergo conformational changes that expose the CARDs and promote homo-oligomerization, cytosol-to-mitochondrion translocation, and interaction with the mitochondrion-localized adaptor molecule MAVS (also called IPS-1, VISA, or CARDIF) (3, 6, 19–21). This interaction initiates a signaling cascade that results in the activation of interferon (IFN) regulatory factor (IRF) family transcription factors, production of type I IFN, expression of cytokines and IFN-stimulated genes (ISGs), and induction of an antiviral state.

RIG-I and MDA5 have been implicated in the control of viral infection in cell culture, with each sensor initiating a host defense response to distinct and overlapping sets of viruses. Picornaviruses, including encephalomyocarditis virus (ECMV), Theiler's murine encephalomyelitis virus (TMEV), and Mengo virus, as well as a calicivirus, murine norovirus, appear to be sensed exclusively by MDA5 (22–24), possibly because the covalently attached Vpg protein on the 5′ end of the viral genome blocks exposure of the 5′-ppp moiety that normally would be recognized by RIG-I. MDA5 also is an important sensor of a coronavirus, murine hepatitis virus (MHV), particularly in the absence of a 2′-O-methylated cap on the viral RNA (25, 26). Furthermore, ectopic expression of MDA5 in human hepatoma cells and fibroblasts inhibited replication of West Nile (WNV) and Venezuelan equine encephalitis viruses (27). In comparison, RIG-I is essential for recognition of hepatitis C (HCV), influenza A, respiratory syncytial, and Sendai (SeV) viruses, whereas RIG-I and MDA5 both serve to recognize infection by WNV and dengue viruses (16, 28). In some cases, MDA5 and RIG-I may function as PRRs with differential kinetics of viral RNA detection, with RIG-I recognizing virus-

or host-generated PAMPs early after infection and MDA5 acting later, after dsRNA viral or host-derived PAMPs accumulate (29, 30).

The importance of RLR signaling for controlling viral pathogenesis is evident from studies with genetically deficient mice. For example, in the absence of MAVS, mice are highly vulnerable to infection with WNV and Sindbis, chikungunya, Coxsackie B (CBV), and rabies viruses (31–36). The contributions of individual RLRs to this response *in vivo* have been more difficult to dissect because the $RIG\text{-}I^{-/-}$ genotype is embryonic lethal on pure genetic backgrounds (e.g., C57BL/6 or 129Sv) (22, 37). $LGP2^{-/-}$ mice are free of developmental defects and exhibited increased susceptibility to WNV infection that was associated with defects in the expansion and fitness of CD8$^+$ T cells (38). $MDA5^{-/-}$ mice develop normally, and their responses to a variety of RNA virus infections have been characterized. $MDA5^{-/-}$ mice had increased mortality, disease severity, and/or viral burden after infection with ECMV, CBV, TMEV, rhinovirus, murine norovirus, SeV, or human metapneumovirus (HMPV) (22–24, 34, 39–43). However, $MDA5^{-/-}$ mice showed no increase in susceptibility to infection with Japanese encephalitis or vesicular stomatitis virus (22).

WNV is a neurotropic flavivirus that is maintained in an enzootic cycle between birds and ornithophillic mosquitoes, with humans and other mammals serving as incidental dead-end hosts (44, 45). It is believed that following subcutaneous inoculation, WNV infects keratinocytes and resident dendritic cells, the latter of which traffic to the draining lymph nodes, where they facilitate spread of infection and development of viremia (46, 47). The mechanism by which WNV crosses the blood-brain barrier (BBB) to infect the central nervous system (CNS) remains unclear, but it may involve passage of virus between compromised cell junctions of the BBB, trafficking of infected leukocytes into the CNS, or direct infection of the microvascular endothelial cells (48, 49). WNV infection causes neurologic injury by direct cytopathic effect on infected neurons, bystander damage to uninfected cells, and immunopathology from infiltrating immune cells responding to the infection (48). In humans, WNV infection can result in encephalitis, meningitis, or flaccid paralysis, and neurologic sequelae may persist even after the infection is resolved (50, 51).

While the innate immune response, especially type I IFN, contributes to the control of virus infection in peripheral tissues, cell-mediated adaptive immunity, particularly CD8$^+$ T cells, restricts and clears WNV infection from the CNS (52–56). Cell culture and *in vivo* studies have established that TLR and RLR signaling orchestrates control of WNV infection (31, 38, 57–61). Although MDA5 contributes to the induction of the antiviral type I IFN response and limits replication of WNV infection in cell culture (27, 29), its contribution to host control of pathogenesis has remained unclear. In this study, we found that while mice lacking MDA5 were more susceptible to WNV infection, the antiviral role of MDA5 *in vivo* was not strongly linked to direct control of viral replication. Rather, a deficiency of MDA5 was associated with functional defects in CD8$^+$ T cells, which resulted in a failure to clear WNV efficiently from CNS tissues.

MATERIALS AND METHODS

Viruses. The WNV strain used (3000.0259) was isolated in New York in 2000 and passaged once in C6/36 *Aedes albopictus* cells to generate a virus stock that was used in all experiments (52, 62). Virus titers were measured by plaque assay on BHK21-15 cells as previously described (52).

Mouse experiments. C57BL/6 wild-type (WT) inbred mice were commercially obtained (Jackson Laboratories, Bar Harbor, ME). $MDA5^{-/-}$ mice (23) were provided by M. Colonna (Washington University, St. Louis, MO) and backcrossed for 10 generations onto a C57BL/6 background. Congenic $CD8^{-/-}$ mice were obtained from Jackson Laboratories. $MDA5^{-/-}$ and $CD8^{-/-}$ mice were genotyped and bred in the animal facilities of the Washington University School of Medicine. $TCR\alpha^{-/-}$ mice were purchased from Jackson Laboratories or were the gift of T. Egawa (Washington University). Nine- to 12-week-old mice were used for all *in vivo* studies except for some of the adoptive-transfer experiments, which used 6-week-old mice. For peripheral infection, 10^2 to 10^4 PFU of WNV was diluted in Hanks balanced salt solution (HBSS) supplemented with 1% heat-inactivated fetal bovine serum (FBS) and inoculated by footpad injection in a volume of 50 μl. For intracranial infection, 10^1 PFU of WNV in a volume of 10 μl was injected into the right cerebral hemisphere. Experiments were approved and performed in accordance with Washington University animal study guidelines.

Tissue viral burden and viremia. To monitor viral spread *in vivo*, mice were infected with 10^2 PFU of WNV by subcutaneous inoculation in the footpad and sacrificed at specified time points (i.e., day 1, 2, 3, 4, 5, 6, 8, or 10) after infection. To monitor viral replication directly in the CNS, mice were infected with 10^1 PFU of WNV by intracranial injection and sacrificed at day 2, 4, or 6 after infection. After extensive cardiac perfusion with phosphate-buffered saline (PBS), organs were harvested, weighed, and homogenized, and virus titers were determined by plaque assay. Viral RNA was isolated from serum using a viral RNA minikit (Qiagen) and measured by fluorogenic quantitative reverse transcription-PCR (qRT-PCR) using primers and probes to the WNV envelope gene (63), One-Step RT-PCR Master Mix, and a 7500 Fast Real-Time PCR System (Applied Biosystems).

Primary cell infections. Cortical neurons were prepared from day 15 mouse embryos, and cerebellar granule cell neurons were prepared from six day-old pups as described previously (64–66). Neurons were seeded in poly-D-lysine–laminin-coated plates (cortical neurons) or poly-D-lysine-coated plates (granule cell neurons) and cultured for 4 days with Neurobasal medium containing B27 supplement, L-glutamine, and penicillin-streptomycin (Invitrogen). Multistep virus growth curves were performed after infection at a multiplicity of infection (MOI) of 0.001, and viral replication was measured by plaque assay.

Quantification of type I IFN activity. Levels of biologically active type I IFN were determined using an ECMV cytopathic effect bioassay performed with L929 cells as described previously (67). Prior to the assay, serum samples were treated with citrate buffer (40 mM citric acid, 10 mM KCl, 135 mM NaCl [pH 3.0]) for 10 min and neutralized with medium containing 45 mM HEPES (pH 8.0). The amount of type I IFN per ml of serum was calculated from a standard curve using alpha interferon (IFN-α; PBL InterferonSource). The IFN specificity of the antiviral activity was confirmed by preincubating L929 cells for 2 h with 25 μg/ml of the IFNAR-blocking monoclonal antibody (MAb) MAR1-5A3 or an isotype control MAb, GIR-208 (68).

Cytokine analysis. Mice were infected subcutaneously with 10^2 PFU of WNV in the footpad, and brains were collected at 8 days after infection following extensive perfusion with PBS. Brains were homogenized in 500 μl of PBS containing 1% heat-inactivated FBS using a Precellys 24 (Bertin Technologies) at 1,500 rpm for 20 s, and cytokines were measured by Luminex array. Protein concentration was assessed by Bradford colorimetric assay (Bio-Rad), and 25 μl of tissue lysate was analyzed using a 13-plex Luminex assay (Millipore) followed by analysis on a Bio-Plex 200 (Bio-Rad). Concentrations of cytokine were normalized to total protein levels. Cytokine levels in serum were measured using a Bio-Plex Pro 23-plex group I cytokine kit (Bio-Rad) and Bio-Plex 200 (Bio-Rad).

Antibody responses. The levels of WNV-specific IgM and IgG were determined using an enzyme-linked immunosorbent assay (ELISA) against purified WNV E protein, as described previously (69).
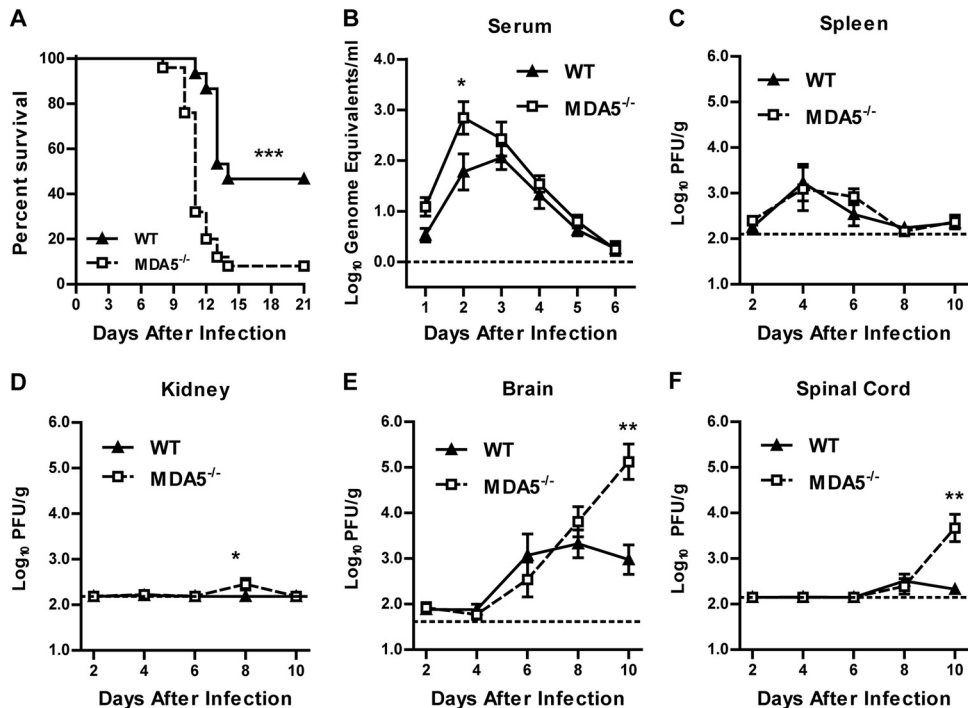
FIG 1 Survival and viral burden in WT and $MDA5^{-/-}$ mice after peripheral inoculation. Mice were infected with 10^2 PFU of WNV in the footpad. (A) Survival was monitored for 21 days in 15 WT and 25 $MDA5^{-/-}$ mice. (B) Viremia was measured by qRT-PCR from 1 to 6 days after infection. (C to F) Viral burden was measured by plaque assay from 2 to 10 days after infection. In panels B to F, results represent means ± SEMs of 7 to 12 mice per group; dotted lines represent the limit of sensitivity of the assay. *, $P < 0.05$; **, $P < 0.01$; ***, $P < 0.001$.

Cellular immune responses. WT and $MDA5^{-/-}$ mice were infected in the footpad with 10^2, 10^3, or 10^4 PFU of WNV, and at 7 days after infection, spleens and brains were harvested after extensive cardiac perfusion with PBS. Splenocytes were dispersed into single-cell suspensions with a cell strainer. Brains were minced and digested with 0.05% collagenase D, 0.1 μg/ml of trypsin inhibitor Nα-p-tosyl-L-lysine chloromethyl ketone, and 10 μg/ml of DNase I in HBSS supplemented with 10 mM HEPES, pH 7.4 (Life Technologies). Cells were dispersed into single-cell suspensions with a cell strainer and pelleted through a 30% Percoll cushion for 30 min (1,200 × g at 4°C). Intracellular IFN-γ or tumor necrosis factor alpha (TNF-α) staining was performed after *ex vivo* restimulation with a D^b-restricted NS4B immunodominant peptide using 1 μM peptide and 5 μg/ml of brefeldin A (Sigma) as described previously (70). Cells were stained with the following antibodies and processed by multicolor flow cytometry on an LSR II flow cytometer (Becton, Dickinson): CD3 (Becton, Dickinson; clone 145-2C11), CD4 (Biolegend; clone RM4-5), CD8β (Biolegend; clone YT5156.7.7), CD25 (eBiosciences; clone PC61.5), FoxP3 (eBiosciences; clone FJK-16S), B220 (Invitrogen), CD45 (Biolegend; clone 30-F11), CD11b (Becton, Dickinson; clone M1/70), CD11c (Becton, Dickinson; clone HL3), CD80 (eBiosciences; clone 16-10A1), CD86 (eBiosciences; clone P03.1), major histocompatibility complex class II (MHC-II; Biolegend; clone M5/114.15.2), CD43 (Biolegend; clone IM7), CD62L (Invitrogen), KLRG1 (Biolegend; clone 2F1/KLRG1), PD1 (Biolegend; RMP1-30), IFN-γ (Becton, Dickinson; clone XMG1.2), TNF-α (Biolegend; clone MP6-XT22), and granzyme B (Invitrogen). Flow cytometry data were analyzed using FlowJo software (Treestar).

Adoptive transfer of primed CD8$^+$ cells. WT and $MDA5^{-/-}$ mice were infected with 10^2 PFU of WNV in the footpad. At 7 days after infection, splenocytes were isolated and CD8$^+$ T cells were purified by positive selection using CD8α microbeads (Miltenyi Biotec). A total of 3×10^6 WT or $MDA5^{-/-}$ donor CD8$^+$ cells were adoptively transferred via an intraperitoneal route to recipient $CD8^{-/-}$ mice that had been infected

with WNV 1 day earlier. A sample of transferred cells was stained with an antibody against CD8α (clone 53-6.7; Becton, Dickinson) or an isotype control and analyzed by flow cytometry (fluorescence-activated cell sorter [FACS] array; Becton, Dickinson) to assess the efficiency of positive selection. WNV-specific CD8$^+$ cells were identified after staining with a D^b-restricted NS4B peptide tetramer, SSVWNATTA (71) (NIH Tetramer Core Facility, Emory University). Nine days following adoptive transfer (10 days after infection), recipient $CD8^{-/-}$ mice were perfused with PBS and viral loads in the brain, spinal cord, and spleen were measured by plaque assay.

Adoptive transfer of naive CD8$^+$ cells. Naive WT and $MDA5^{-/-}$ splenocytes were purified by positive selection using CD8α or CD4 microbeads and an autoMACS Pro Separator (Miltenyi Biotec). A total of 1×10^7 WT or $MDA5^{-/-}$ CD8$^+$ cells plus 2×10^6 WT CD4$^+$ cells were transferred to recipient $TCR\alpha^{-/-}$ mice by an intravenous route. One day following transfer, recipient mice were infected with 10^2 PFU of WNV in the footpad. At 9 days following infection (10 days after transfer), recipient mice (and no-transfer controls) were perfused with PBS and brains were processed as described above. Cells were stained with the following antibodies and processed by multicolor flow cytometry on an LSR II flow cytometer (Becton, Dickinson): CD3 (Becton, Dickinson; clone 145-2C11), CD4 (Biolegend; clone RM4-5), CD8α (Biolegend; clone 53-6.7), CD19 (Biolegend; clone 6D5), and granzyme B (Invitrogen). WNV-specific CD8$^+$ cells were identified after staining with the D^b-restricted NS4B peptide tetramer. Flow cytometry data were analyzed using FlowJo software (Treestar).

Statistical analysis. Viral growth curves were analyzed by a 2-way analysis of variance (ANOVA). For viral burden, serum bioassay, antibody, and lymphocyte analyses, differences were analyzed by the Mann-Whitney test. Kaplan-Meier survival curves were analyzed by the log rank test. All data were analyzed using Prism software (GraphPad Prism 5; GraphPad, San Diego, CA).
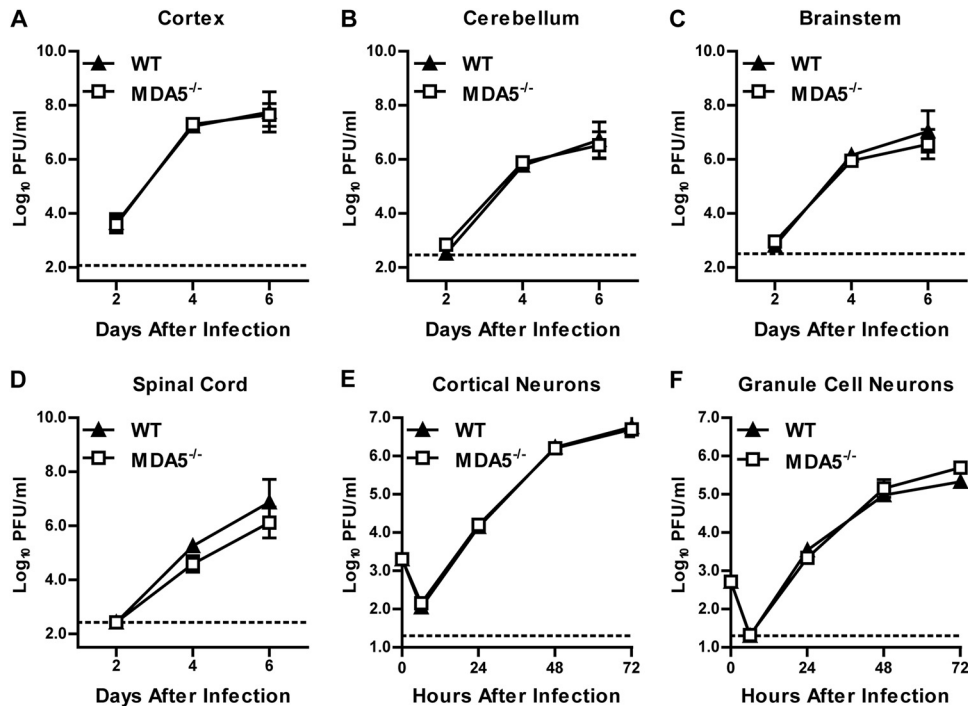
FIG 2 Viral replication in CNS tissues and cells from WT and $MDA5^{-/-}$ mice. (A to D) Mice were infected with 10^1 PFU of WNV by intracranial injection. Viral replication was measured by plaque assay from 2 to 6 days after infection. Results represent means ± SEMs of 6 to 10 mice per group; dotted lines represent the limit of sensitivity of the assay. (E and F) Multistep growth curves in cortical neurons and cerebellar granule cell neurons. Cells were infected at an MOI of 0.001 for 72 h, and viral replication was measured by plaque assay. Results represent means ± SEMs of 6 samples from 2 independent experiments; dotted lines represent the limit of sensitivity of the assay.

RESULTS

Susceptibility of $MDA5^{-/-}$ mice to WNV infection. To determine if MDA5 is necessary for restricting WNV pathogenesis *in vivo*, we infected WT and $MDA5^{-/-}$ mice with WNV by subcutaneous inoculation and monitored survival over time. $MDA5^{-/-}$ mice exhibited enhanced mortality (92% versus 53%; $P < 0.001$) (Fig. 1A) and reduced average survival time (mean times to death, 11.1 and 12.8 days for $MDA5^{-/-}$ and WT mice, respectively; $P < 0.01$) compared to infected WT mice. To determine the basis for this increased lethality, we measured viral loads in tissues following WNV infection. We found that MDA5 was largely dispensable for controlling WNV replication in peripheral organs, as $MDA5^{-/-}$ mice showed only a small increase in viremia at a single time point (11-fold greater at day 2 after infection; $P < 0.05$) (Fig. 1B). In comparison, no significant differences were observed in viral burden in the spleen (Fig. 1C), and only limited replication in the kidneys was detected in 5 of 12 $MDA5^{-/-}$ mice (at 8 days after infection; $P < 0.05$) (Fig. 1D). These results were unanticipated given the marked increase in viremia and visceral organ infection observed in $MAVS^{-/-}$ mice, which completely lack RLR signaling (31), and the increased viral loads observed when $MDA5^{-/-}$ mice were infected with other RNA viruses (22, 24, 39–43).

Consistent with a small effect of MDA5 on controlling WNV infection in peripheral tissues, early entry into the CNS was not observed in $MDA5^{-/-}$ mice compared to WT controls. Similar levels of WNV were observed at days 2 through 8 in the brain and spinal cord ($P > 0.05$), but $MDA5^{-/-}$ mice exhibited marked increases in viral titers in the CNS at later times after infection. At day 10 after infection, we observed a 140-fold-higher viral burden

in the brain ($P < 0.01$) (Fig. 1E) and a 21-fold-higher viral burden in the spinal cord ($P < 0.01$) (Fig. 1F) in $MDA5^{-/-}$ mice than in WT controls. These results suggest that MDA5 is important in controlling immunity to WNV in the CNS.

Because previous studies showed direct antiviral effects of the RLR signaling pathway in cells of the CNS (43), we hypothesized that the enhanced WNV infection phenotype in $MDA5^{-/-}$ mice could be explained by an MDA5-dependent restriction of replication in neuronal cells. To test this, wild-type and $MDA5^{-/-}$ mice were infected with 10^1 PFU of WNV directly into the brain via an intracranial route, and viral burden in the cerebral cortex, brain stem, cerebellum, and spinal cord was measured on days 2, 4, and 6 after infection. In contrast to the increased viral titers observed in the CNS of $MDA5^{-/-}$ mice after peripheral inoculation, we observed no differences in infection between WT and $MDA5^{-/-}$ mice following intracranial injection ($P > 0.05$) (Fig. 2A to D). Consistent with this, an absence of MDA5 did not impact WNV infection in primary cortical or cerebellar neuron cultures ($P > 0.05$) (Fig. 2E and F).

Effect of MDA5 on innate immune responses *in vivo*. One explanation for the increased viral load in the CNS of $MDA5^{-/-}$ mice after subcutaneous infection might be a defective MDA5-dependent protective immune response originating in the periphery. As MDA5 contributes to the induction of type I IFN *in vivo* in the context of multiple viral infections (22, 34, 39–43, 72, 73) and to the induction of ISGs after WNV infection in fibroblasts (29), we assessed the impact of the loss of MDA5 on systemic levels of type I IFN after WNV infection (Fig. 3A). Contrary to what has been reported with other viral infections, we did not observe a
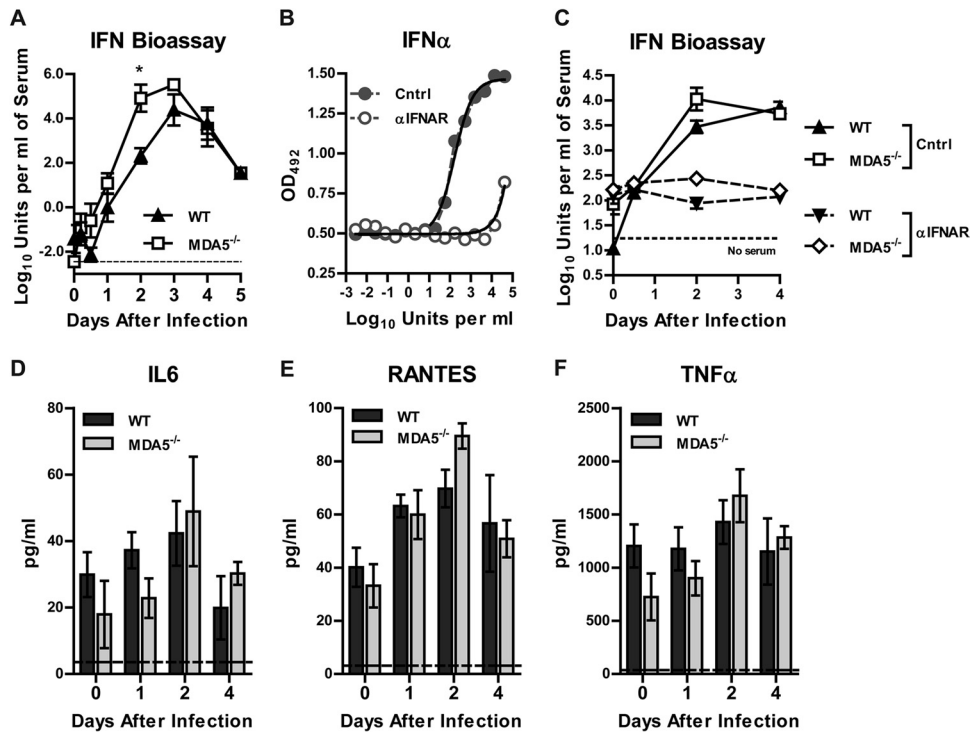
FIG 3 Type I IFN and inflammatory responses to WNV infection in WT and $MDA5^{-/-}$ mice. Mice were infected with 10^2 PFU of WNV in the footpad. (A) Type I IFN activity in serum was measured by an ECMV cytopathic effect bioassay. (B) Cells were incubated with an anti-IFNAR or control MAb prior to treatment with IFN-α and ECMV infection. Cell survival was measured by a colorimetric assay. OD_{492}, optical density at 492 nm. (C) Cells were incubated with an anti-IFNAR or control MAb prior to measurement of type I IFN activity in serum by ECMV cytopathic effect bioassay. (D to F) Cytokine and chemokine levels in serum were measured by Bio-Plex assay. Results represent means ± SEMs of 5 mice per group; dotted lines represent the limit of sensitivity of the assay.*, $P < 0.05$.

deficiency in type I IFN levels in the serum of $MDA5^{-/-}$ mice. Moreover, by 2 days after infection, $MDA5^{-/-}$ mice had higher levels (396-fold; $P < 0.05$) of type I IFN in serum than did WT mice, possibly driven by the increased viremia at this time point. We confirmed that the observed serum antiviral activity was due to type I IFN, as it was completely neutralized by an IFNAR-blocking antibody (Fig. 3B and C). Although MDA5 contributes to inflammatory cytokine production in the context of other viral infections (24, 40, 41), we did not detect a significant difference between WT and $MDA5^{-/-}$ mice in levels of 23 cytokines and chemokines in serum at day 0, 1, 2, or 4 after infection (Fig. 3D to F and Table 1).

While MDA5 did not modulate cytokine or chemokine production systemically, we hypothesized that MDA5 might regulate production in the CNS in a manner that is required for WNV control. To assess this, we infected WT and $MDA5^{-/-}$ mice subcutaneously and measured the levels of nine cytokines and chemokines in the brain at day 8 after infection (Fig. 4). Notably, we failed to detect any deficit in cytokine production in the brains of $MDA5^{-/-}$ mice. While there was no difference in macrophage inflammatory protein 1 (MCP-1), MIP-1α, interleukin 1α (IL-1α), IL-6, or IFN-γ production, levels of MIP-1β, IL-12 (p70), RANTES, and TNF-α were in fact greater in $MDA5^{-/-}$ mice than in WT mice, likely secondary to enhanced viral replication in the brains of $MDA5^{-/-}$ mice.

Effect of MDA5 on adaptive immune responses *in vivo*. Our prior studies revealed an innate/adaptive immune interface that

was regulated by MAVS and modulated the magnitude of the humoral immune response to WNV infection (31). To assess the effect of MDA5 on WNV-specific antibody responses, we analyzed serum from $MDA5^{-/-}$ and WT mice 4, 6, and 8 days after infection for binding to WNV E protein. We observed no defects in anti-WNV E protein IgM or IgG responses in $MDA5^{-/-}$ mice (Fig. 5). Indeed, we observed a small increase in WNV-specific IgM titers in $MDA5^{-/-}$ mice at 6 days after infection, again possibly reflecting the slightly increased viremia observed in these mice. Thus, the difference in WNV pathogenesis in $MDA5^{-/-}$ mice did not appear to be explained by altered humoral immune responses.

We next considered whether defects in cellular immune responses in $MDA5^{-/-}$ mice could explain their susceptibility to WNV infection. This seemed a plausible hypothesis, as mice deficient in CD8 or perforin showed an analogous late-stage phenotype in the CNS (53, 74), and $LGP2^{-/-}$ mice exhibited defects in $CD8^+$ T cell immunity during viral infection (38). Additional studies suggest that MDA5-dependent responses to soluble PAMPs or lymphocytic choriomeningitis virus (LCMV) infection can boost induction of effector and memory $CD8^+$ T cell subsets (73, 75). We harvested splenocytes from WT and $MDA5^{-/-}$ mice 7 days after WNV infection and performed immunophenotyping analysis. Cells were stained with antibodies to detect T cells (CD3, CD4, and CD8), their migratory capacity (CD43 and CD62L), state of differentiation or exhaustion (KLRG1 and PD1), and production of effector molecules (IFN-γ, TNF-α, and granzyme B)

TABLE 1 Serum cytokine levels after WNV infection of WT and $MDA5^{-/-}$ mice[a]

		Value on indicated day postinfection[a]											
		0			1			2			4		
		Cytokine level (pg/ml)			Cytokine level (pg/ml)			Cytokine level (pg/ml)			Cytokine level (pg/ml)		
Cytokine	LOD[b]	WT	$MDA5^{-/-}$	P	WT	$MDA5^{-/-}$	P	WT	$MDA5^{-/-}$	P	WT	$MDA5^{-/-}$	P
IL-1α	19.2	55.1 (8.1)	41.6 (3.5)	0.16	70.7 (6.8)	49.4 (4.6)	0.03	55.6 (4.2)	64.7 (9.9)	0.42	47.2 (5.1)	72.3 (15.2)	0.20
IL-1β	37.4	431.2 (101.1)	407.1 (132.4)	0.89	476.2 (55.6)	277.9 (105.5)	0.14	373.2 (147.9)	533.4 (50.5)	0.34	402.5 (126.6)	647.4 (69.2)	0.11
IL-2	49.9	164.2 (23.2)	133.6 (20.0)	0.35	163.1 (19.2)	148.0 (23.3)	0.63	173.7 (15.7)	177.3 (21.6)	0.90	152.8 (37.4)	150.0 (12.1)	0.94
IL-3	1.4	16.0 (4.7)	7.6 (4.2)	0.22	16.1 (6.7)	12.9 (4.6)	0.70	20.5 (4.2)	20.2 (6.3)	0.96	17.4 (9.3)	18.7 (3.9)	0.90
IL-4	5.4	5.4 (0.0)	5.4 (0.0)	1.00	5.4 (0.0)	5.4 (0.0)	1.00	5.4 (0.0)	5.4 (0.0)	1.00	5.4 (0.0)	5.4 (0.0)	1.00
IL-5	11.5	124.9 (28.6)	61.7 (30.2)	0.17	114.3 (30.6)	92.8 (27.4)	0.61	135.6 (20.7)	127.9 (23.0)	0.81	101.5 (49.0)	119.5 (18.6)	0.72
IL-6	3.6	29.9 (6.8)	17.9 (10.1)	0.35	37.3 (5.4)	22.8 (6.0)	0.11	42.3 (9.7)	48.9 (16.5)	0.74	19.9 (9.5)	30.3 (3.4)	0.30
IL-9	80.1	225.4 (89.1)	184.4 (50.6)	0.70	230.6 (32.8)	183.4 (57.9)	0.50	248.8 (74.2)	315.4 (65.3)	0.52	178.7 (87.2)	195.0 (70.8)	0.89
IL-10	11.4	186.2 (57.5)	70.0 (24.6)	0.10	182.0 (45.6)	128.9 (35.1)	0.38	206.7 (43.7)	218.7 (29.1)	0.83	166.5 (73.7)	202.3 (24.9)	0.63
IL-12 (p40)	16.4	143.5 (19.9)	156.5 (27.7)	0.71	151.5 (9.8)	119.1 (15.3)	0.11	172.1 (19.5)	207.2 (16.1)	0.20	174.9 (32.0)	155.5 (18.0)	0.59
IL-12 (p70)	27.1	176.1 (30.4)	104.6 (33.5)	0.15	160.7 (21.7)	141.4 (22.9)	0.56	195.5 (29.5)	214.8 (29.3)	0.65	155.9 (47.3)	188.9 (14.5)	0.48
IL-13	95.0	394.2 (101.5)	207.9 (113.0)	0.25	284.1 (126.3)	212.1 (60.1)	0.62	393.0 (113.7)	365.1 (123.0)	0.87	345.0 (152.9)	421.4 (96.8)	0.67
IL-17	10.2	90.3 (20.4)	40.7 (22.5)	0.14	83.9 (18.5)	84.0 (21.0)	1.00	124.2 (20.3)	146.4 (10.1)	0.36	87.9 (24.0)	118.3 (11.5)	0.26
Eotaxin	64.3	729.5 (242.7)	862.9 (311.5)	0.74	996.9 (362.9)	758.4 (272.1)	0.61	813.2 (308.0)	1,181.6 (260.5)	0.39	777.7 (445.7)	949.7 (282.5)	0.74
G-CSF[c]	48.2	218.2 (63.4)	115.3 (27.1)	0.17	200.8 (20.1)	182.0 (32.7)	0.64	162.4 (27.0)	181.2 (50.5)	0.75	147.0 (33.6)	170.9 (12.1)	0.49
GM-CSF[d]	18.2	347.8 (101.4)	316.4 (118.2)	0.85	529.2 (91.5)	378.0 (125.6)	0.36	422.9 (128.8)	556.4 (76.7)	0.40	422.7 (162.7)	544.1 (61.7)	0.47
IFN-γ	6.3	6.3 (0.0)	6.3 (0.0)	1.00	6.3 (0.0)	6.3 (0.0)	1.00	6.3 (0.0)	6.3 (0.0)	1.00	6.3 (0.0)	6.3 (0.0)	1.00
KC	9.1	159.3 (52.5)	238.6 (131.9)	0.59	111.6 (11.8)	99.7 (25.6)	0.59	105.9 (20.0)	136.9 (30.7)	0.42	112.9 (29.7)	150.1 (20.8)	0.33
MCP-1	75.2	334.5 (73.7)	171.8 (86.1)	0.19	319.6 (73.5)	268.8 (60.2)	0.19	444.0 (91.1)	450.8 (121.8)	0.97	345.2 (157.6)	442.1 (87.3)	0.59
MIP-1α	10.1	36.5 (8.1)	24.6 (7.9)	0.32	34.8 (5.2)	32.3 (10.5)	0.83	33.3 (7.2)	57.9 (17.8)	0.24	22.2 (7.4)	27.8 (3.6)	0.49
MIP-1β	31.9	254.7 (64.5)	102.5 (70.6)	0.15	333.7 (65.6)	214.3 (61.5)	0.15	343.1 (49.5)	510.8 (171.8)	0.38	256.9 (113.1)	320.9 (37.5)	0.57
RANTES	3.1	40.2 (7.3)	33.2 (8.2)	0.54	63.2 (4.3)	59.9 (9.2)	0.54	69.7 (7.1)	89.5 (4.7)	0.05	56.6 (18.2)	50.9 (7.0)	0.75
TNF-α	36.3	1,204.7 (202.3)	724.5 (220.2)	0.15	1,177.3 (202.2)	900.7 (162.3)	0.15	1,428.7 (205.4)	1,676.2 (247.6)	0.46	1,151.8 (311.6)	1,283.6 (106.4)	0.67

[a] Mice were infected with 10^2 PFU of WNV in the footpad. Serum was collected at 1, 2, and 4 days after infection and from naive mice (day 0), and the indicated cytokines were measured by Bio-Plex array. Data represent the means (SEMs) of 5 mice per group.
[b] LOD, limit of detection.
[c] G-CSF, granulocyte colony-stimulating factor.
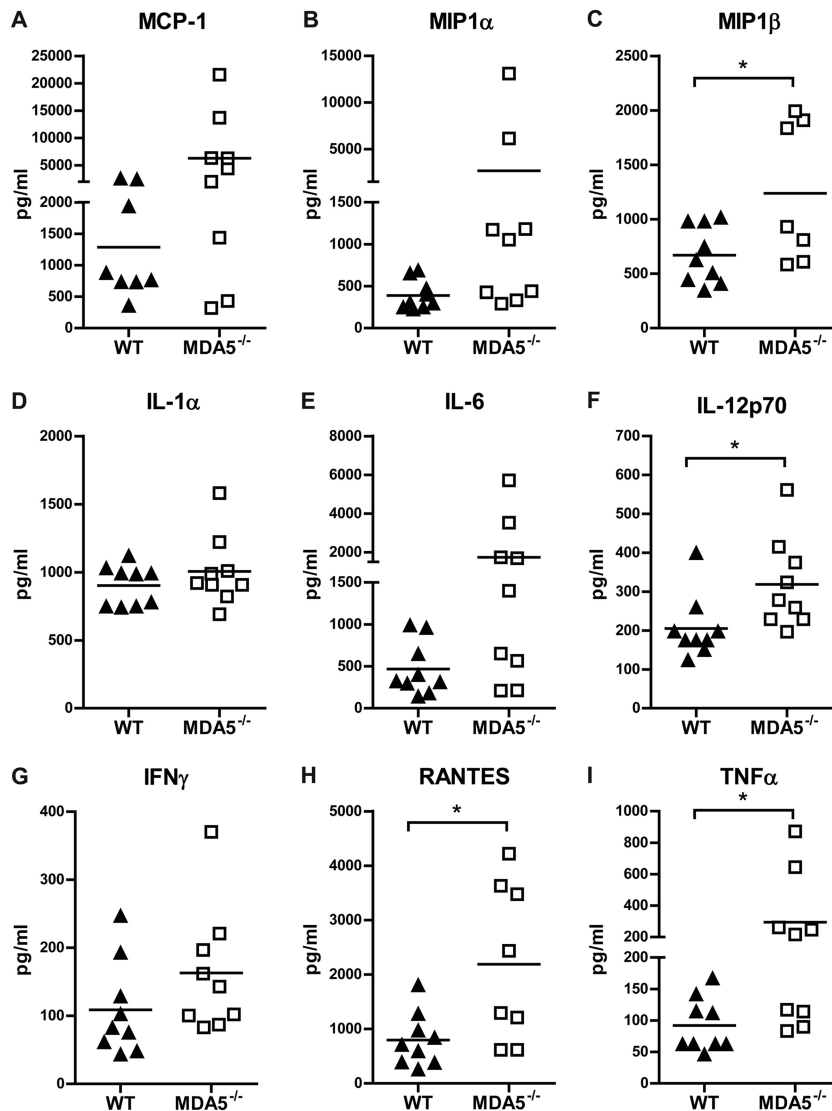[d] GM-CSF, granulocyte-macrophage colony-stimulating factor.

FIG 4 Cytokine expression in brains of WNV-infected WT and *MDA5*^{−/−} mice. Mice were infected with 10^2 PFU of WNV in the footpad. Brains were harvested at 8 days after infection, and the indicated cytokines and chemokines were assessed by Luminex array. Data are shown as the means ± SEMs of 9 mice per group. *, $P < 0.05$.
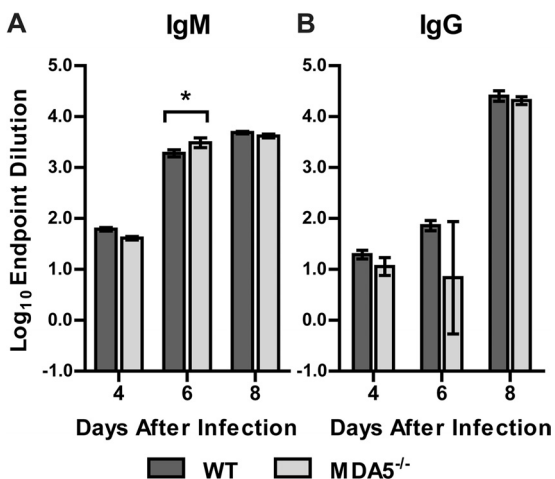

FIG 5 Antibody responses in infected WT and *MDA5*^{−/−} mice. Serum IgM (A) and IgG (B) against WNV E protein were measured by ELISA. Results represent the means ± SEMs of 6 to 10 mice per group. *, $P < 0.05$.

after WNV peptide restimulation. In addition, we measured antigen-presenting cells and their state of activation (B220, CD45, CD11b, CD11c, CD80, CD86, and MHC-II) as well as regulatory T cells (CD25 and FoxP3). Notably, we observed no marked differences in the quality and quantity of these leukocyte responses between WT and *MDA5*^{−/−} mice after WNV infection (Fig. 6 and Tables 2 and 3), even when 10- or 100-fold-higher doses of virus were used (data not shown). In general, there was little difference in the numbers or percentages of WNV-specific CD8^{+} T cells. We did observe, however, higher KLRG1 and CD62L expression on *MDA5*^{−/−} CD8^{+} IFN-γ^{+} and CD8^{+} TNF-α^{+} cells, suggesting that there may be some functional differences compared to WT cells.

Although leukocyte function appeared relatively intact in spleens from *MDA5*^{−/−} mice, it remained possible that the virologic phenotype in the CNS was due to impaired leukocyte trafficking across the BBB or altered function of cells within the CNS. Therefore, we performed a similar analysis on leukocytes in the
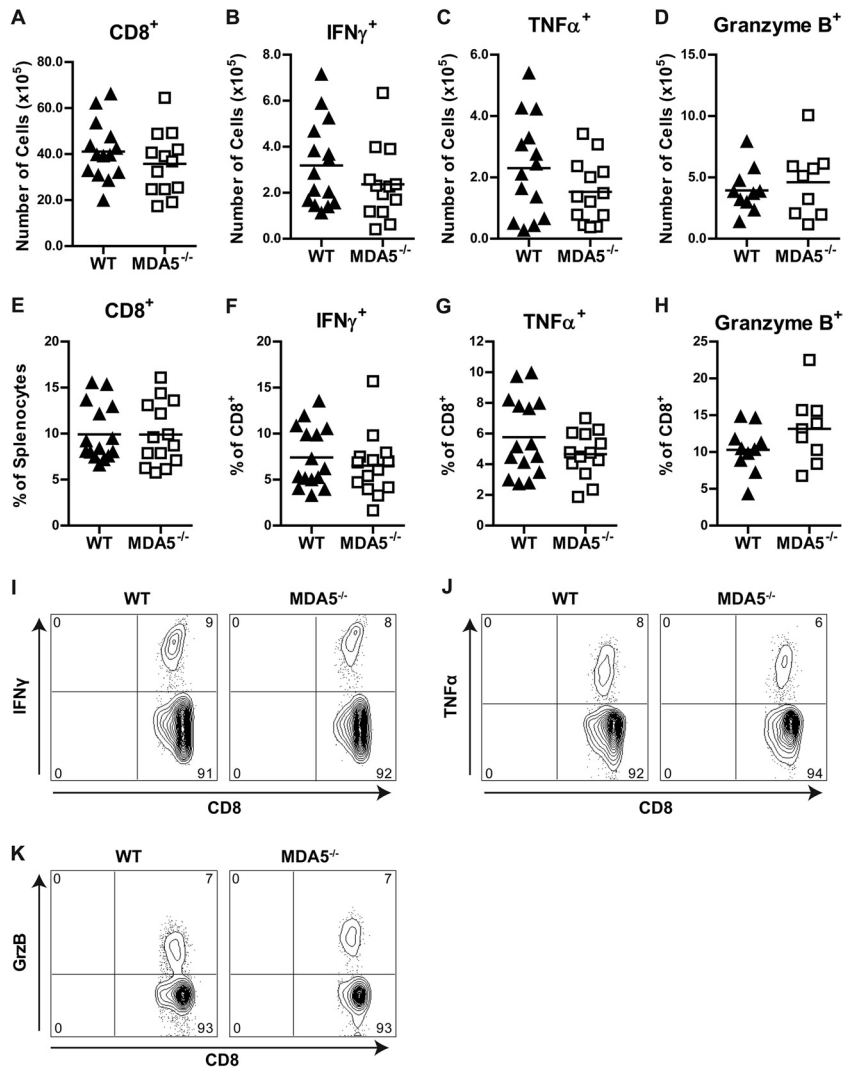
FIG 6 (A to H) Immunophenotyping of splenocytes from infected WT and $MDA5^{-/-}$ mice. Mice were infected with 10^2 PFU of WNV in the footpad. Splenocytes were harvested and analyzed by flow cytometry at 7 days after infection. Numbers (A to D) and percentages (E to H) of the indicated populations are shown; symbols represent individual mice. CD8$^+$, IFN-γ^+, and TNF-α^+ populations represent cells that were restimulated with an immunodominant WNV peptide. (I to K) Representative flow cytometry plots of IFN-γ^+, TNF-α^+, and granzyme B$^+$ cell populations. Numbers indicate the percentage of cells in each quadrant.

brain at day 7 after WNV infection. Again, relatively few differences were observed in the infiltrating immune cells in the brains of $MDA5^{-/-}$ mice compared to WT mice (Fig. 7 and Tables 4 and 5), and higher infecting doses of WNV did not reveal any marked

changes (data not shown). There was no significant difference in the number or percentage of WNV-specific CD8$^+$ T cells in the brain, although $MDA5^{-/-}$ mice had higher numbers and percentages of CD45$^+$ CD11b$^+$ macrophages. One notable difference was

TABLE 2 Phenotypes of splenocytes in WT and $MDA5^{-/-}$ mice after WNV infection[a]

Phenotype	Total no. of cells			% of gated cells			Type of gated cell
	WT	$MDA5^{-/-}$	P	WT	$MDA5^{-/-}$	P	
CD4$^+$	2.3×10^7 (2.2×10^6)	2.3×10^7 (2.0×10^6)	0.86	16.8 (0.7)	16.9 (1.1)	0.98	Splenocytes
CD4$^+$ CD25$^+$ FoxP3$^+$	2.5×10^6 (3.3×10^5)	2.6×10^6 (2.8×10^5)	0.78	10.2 (0.6)	11.6 (0.6)	0.12	CD4$^+$ T cells
CD8$^+$	4.1×10^6 (3.4×10^5)	3.6×10^6 (3.8×10^5)	0.30	9.9 (0.8)	9.9 (0.9)	0.99	Splenocytes
IFN-γ^+	3.2×10^5 (4.8×10^4)	2.4×10^5 (4.5×10^4)	0.23	7.4 (0.9)	6.5 (0.9)	0.47	CD8$^+$ T cells
TNF-α^+	2.0×10^5 (4.3×10^4)	1.5×10^5 (2.8×10^4)	0.15	5.8 (0.7)	4.7 (0.4)	0.18	CD8$^+$ T cells
Granzyme B$^+$	4.0×10^5 (5.8×10^4)	4.6×10^5 (9.3×10^4)	0.55	10.3 (1.0)	13.1 (1.6)	0.14	CD8$^+$ T cells

[a] Mice were infected with 10^2 PFU of WNV in the footpad. Splenocytes were harvested and analyzed by flow cytometry at day 7 after infection. Numbers and percentages of the indicated populations are shown as means (SEMs) of approximately 15 mice per group. CD8$^+$, IFN-γ^+, and TNF-α^+ populations represent cells that were restimulated with an immunodominant WNV peptide.

TABLE 3 Phenotypes of antigen-specific CD8$^+$ T cells in the spleens of WT and $MDA5^{-/-}$ mice after WNV infection[a]

Phenotype	Fluorescence intensity within IFN-γ$^+$ cells			Fluorescence intensity within TNF-α$^+$ cells		
	WT	$MDA5^{-/-}$	P	WT	$MDA5^{-/-}$	P
KLRG1	102.2 (3.5)	132.0 (5.2)	0.00005*	100.3 (3.2)	117.9 (7.9)	0.044*
PD1	102.9 (4.4)	123.3 (9.1)	0.05	96.3 (3.0)	108.3 (6.8)	0.11
CD43	104.5 (6.8)	110.4 (8.7)	0.59	100.4 (5.9)	92.1 (5.2)	0.30
CD62L	103.3 (4.5)	112.8 (6.7)	0.24	111.0 (9.2)	138.5 (9.7)	0.049*

[a] Mice were infected with 10^2 PFU of WNV in the footpad. Splenocytes were harvested and analyzed by flow cytometry at 7 days after infection. Values indicate the geometric mean fluorescence intensity of the indicated phenotypic marker within IFN-γ$^+$ or TNF-α$^+$ populations, shown as means (SEMs) of approximately 15 mice per group. Asterisk indicates significant differences between WT and $MDA5^{-/-}$ cells.

that CD8$^+$ IFN-γ$^+$ and CD8$^+$ TNF-α$^+$ cells from the brains of $MDA5^{-/-}$ mice had higher expression of the exhaustion marker PD1 than did cells from WT mice. Nonetheless, $MDA5^{-/-}$ WNV-specific CD8$^+$ T cells in the brain had no relative change in the expression of KLRG1, CD43, CD62L, IFN-γ, or TNF-α. We also examined the localization of CD3$^+$ cells in the brains of infected WT and $MDA5^{-/-}$ mice by confocal microscopy. In the cerebral cortex and cerebellum, $MDA5^{-/-}$ T cells were present in the parenchyma and showed no evidence of perivascular retention (data not shown), indicating that the increased CNS titers observed in $MDA5^{-/-}$ mice were not due to impaired trafficking of the antigen-specific T cells responsible for CNS clearance.

Adoptive-transfer experiments. While priming in the periph-

ery and trafficking of antigen-specific CD8$^+$ T cells into the brains of $MDA5^{-/-}$ mice appeared normal, we observed subtle differences in some phenotypic markers, which in theory could influence virus clearance. To establish the role of MDA5 in T cell priming or effector activity, we performed two adoptive-transfer experiments. In the first experiment, WNV-primed CD8$^+$ T cells from WT and $MDA5^{-/-}$ mice were transferred into infected $CD8^{-/-}$ mice, allowing us to assess the function in a common $MDA5^{+/+}$ environment of cells that were primed in the presence or absence of MDA5. In the second experiment, we transferred naive WT or $MDA5^{-/-}$ CD8$^+$ T cells to assess their function when primed in a common $MDA5^{+/+}$ environment.

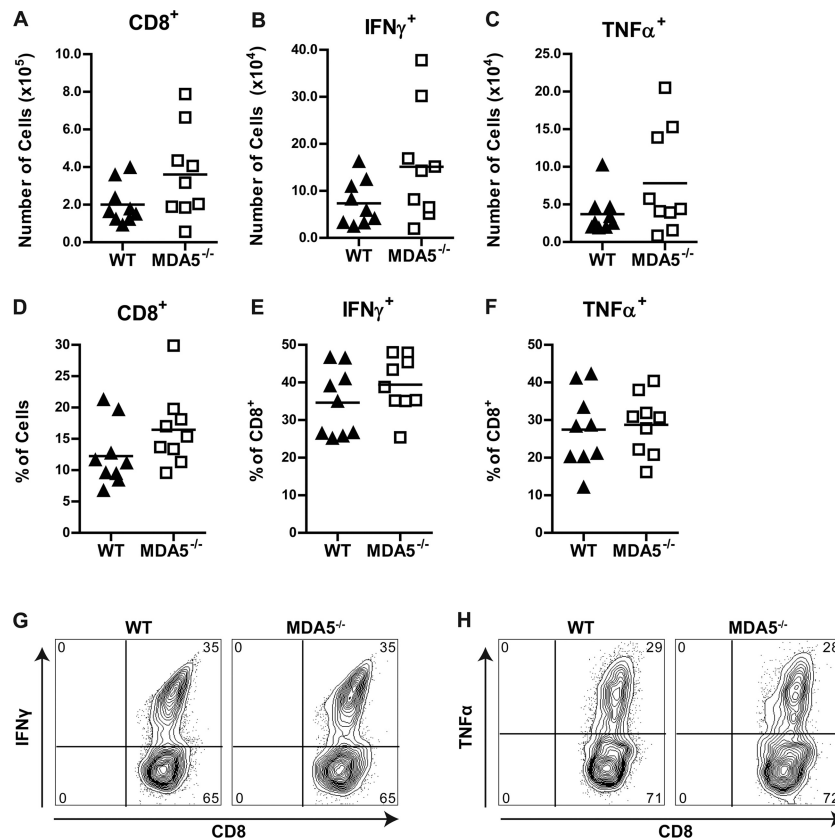To test whether CD8$^+$ T cells primed in an $MDA5^{-/-}$ environ-

FIG 7 (A to F) Immunophenotyping of brain leukocytes in infected WT and $MDA5^{-/-}$ mice. Mice were infected with 10^2 PFU of WNV in the footpad. Brains were harvested and analyzed by flow cytometry at 7 days after infection. Numbers (A to C) and percentages (D to F) of the indicated populations are shown; symbols represent individual mice. CD8$^+$, IFN-γ$^+$, and TNF-α$^+$ populations represent cells that were restimulated with an immunodominant WNV NS4B peptide. (G and H) Representative flow cytometry plots of IFN-γ$^+$ and TNF-α$^+$ populations. Numbers indicate the percentage of cells in each quadrant.

TABLE 4 Phenotypes of brain leukocytes in WT and $MDA5^{-/-}$ mice after WNV infection[a]

| | Total no. of cells | | | Percentage of gated cells | | | |
Phenotype	WT	$MDA5^{-/-}$	P	WT	$MDA5^{-/-}$	P	Type of gated cell
CD4^{+}	9.4×10^4 (1.4×10^4)	1.1×10^5 (1.8×10^4)	0.47	5.8 (0.6)	5.5 (0.6)	0.72	Total
CD4^{+} CD25^{+} FoxP3^{+}	5.1×10^3 (1.2×10^3)	7.9×10^3 (2.4×10^3)	0.31	5.4 (1.0)	6.6 (1.0)	0.39	CD4^{+} T cells
CD8^{+}	2.0×10^5 (3.6×10^4)	3.6×10^5 (8.0×10^4)	0.09	12.3 (1.7)	16.5 (2.0)	0.12	Total
IFN-γ^{+}	7.4×10^4 (1.6×10^4)	1.5×10^5 (4.0×10^4)	0.09	34.6 (3.0)	39.4 (2.5)	0.24	CD8^{+} T cells
TNF-α^{+}	3.7×10^4 (8.9×10^3)	7.8×10^4 (2.3×10^4)	0.12	27.5 (3.4)	28.8 (2.7)	0.76	CD8^{+} T cells
CD45^{lo} CD11b^{+} (microglia)	4.2×10^5 (7.2×10^4)	4.5×10^5 (9.8×10^4)	0.80	24.1 (2.9)	19.0 (1.7)	0.16	Total
CD45^{hi} CD11b^{+} (macrophages)	3.3×10^5 (3.8×10^4)	6.1×10^5 (1.1×10^5)	0.03*	18.6 (2.0)	27.3 (0.9)	0.002*	Total

[a] Mice were infected with 10^2 PFU of WNV in the footpad. Brains were harvested and analyzed by flow cytometry at 7 days after infection. Numbers and percentages of the indicated populations are shown as means (SEMs) of 8 mice per group. CD8^{+}, IFN-γ^{+}, and TNF-α^{+} populations represent cells that were restimulated with an immunodominant WNV peptide. Asterisk indicates significant differences between WT and $MDA5^{-/-}$ cells.

ment were functionally equivalent to their WT counterparts, we isolated primed donor CD8^{+} T cells from WT and $MDA5^{-/-}$ mice at 7 days after WNV infection and transferred them into recipient $CD8^{-/-}$ mice that had been infected with WNV 1 day earlier. We confirmed that WNV-infected WT and $MDA5^{-/-}$ mice had equivalent percentages of CD8^{+} splenocytes (Fig. 8A), that this proportion was enriched following positive selection (Fig. 8B), and that similar numbers and percentages of antigen-specific WT and $MDA5^{-/-}$ CD8^{+} T cells were transferred (Fig. 8C). Nine days following adoptive transfer (10 days after WNV infection), we measured tissue viral loads in recipient $CD8^{-/-}$ mice. Although mice that received WT CD8^{+} T cells had no detectable WNV in the CNS or the spleen, those receiving $MDA5^{-/-}$ CD8^{+} T cells failed to control CNS infection even though virus was cleared from the spleen (Fig. 8D). These results demonstrate that CD8^{+} T cells primed in $MDA5^{-/-}$ mice have functional deficits relative to cells primed in WT mice. This produces a cell-intrinsic defect of $MDA5^{-/-}$ CD8^{+} T cells that results in an inability to clear WNV infection in the CNS, even when transferred into an $MDA5^{+/+}$ environment.

What remained unclear was whether the defect of $MDA5^{-/-}$ CD8^{+} T cell function was cell autonomous and due to a direct requirement for MDA5 in the T cell itself or non-cell autonomous and due to a defective $MDA5^{-/-}$ priming environment. To address this, we isolated naive CD8^{+} T cells from WT and $MDA5^{-/-}$ mice and transferred them into $MDA5^{+/+}$ animals prior to WNV infection. As transfers of naive cells into $CD8^{-/-}$ mice were inefficient (data not shown), we used $TCR\alpha^{-/-}$ mice as recipients. Along with CD8^{+} cells, we also transferred naive WT CD4^{+} cells, as $TCR\alpha^{-/-}$ mice lack both CD8^{+} and CD4^{+} cells, and CD4-

mediated help is necessary for sustaining CD8-mediated clearance of WNV from the CNS (76). One day following adoptive transfer, recipient mice were infected with WNV and infiltrating lymphocytes were assessed in the brain at 9 days after infection. We detected equivalent percentages and numbers of CD8^{+} and WNV antigen-specific cells in the brains of mice receiving WT versus $MDA5^{-/-}$ CD8^{+} cells (Fig. 9A and B and data not shown). Furthermore, we did not detect any significant difference in expression of phenotypic markers, including CD43, PD1, KLRG1, or granzyme B, in the recipient mice (Fig. 9C and data not shown). These observations imply that WT and $MDA5^{-/-}$ CD8^{+} cells are phenotypically equivalent after priming in an $MDA5^{+/+}$ environment. Our results suggest that the inability of $MDA5^{-/-}$ CD8^{+} cells to control WNV infection in the CNS in $MDA5^{-/-}$ mice reflects a non-cell-autonomous role for MDA5 in proper CD8^{+} T cell priming.

DISCUSSION

While prior studies established that RLR signaling is critical for controlling WNV pathogenesis (31), the relative contributions of RIG-I and MDA5 to sensing WNV infection and coordinating innate and adaptive immune responses *in vivo* have remained unclear. Here, we established that in the context of WNV infection, an absence of MDA5 *in vivo* resulted in increased lethality and higher viral loads in the CNS than in WT mice. Somewhat unexpectedly, MDA5 did not have a dominant direct role in restricting viral replication in peripheral tissues or neurons, and the systemic IFN response to WNV remained intact. Instead, the increased WNV titers in the CNS of $MDA5^{-/-}$ mice were linked to a qualitative defect of $MDA5^{-/-}$ CD8^{+} T cells in clearing infection from

TABLE 5 Phenotype of antigen-specific CD8^{+} T cells in the brains of WT and $MDA5^{-/-}$ mice after WNV infection[a]

| | Fluorescence intensity within CD8^{+} cells | | | Fluorescence intensity within IFN-γ^{+} cells | | | Fluorescence intensity within TNF-α^{+} cells | | |
Phenotype	WT	$MDA5^{-/-}$	P	WT	$MDA5^{-/-}$	P	WT	$MDA5^{-/-}$	P
IFN-γ[+]	98.4 (4.9)	107.0 (5.1)	0.24						
TNF-α[+]	94.2 (6.3)	98.5 (7.4)	0.67						
KLRG1				100.2 (5.8)	109.1 (6.2)	0.31	99.4 (6.0)	104.0 (5.3)	0.57
PD1				102.6 (5.2)	140.1 (13.1)	0.02*	101.7 (5.3)	146.4 (15.7)	0.02*
CD43				100.3 (4.9)	112.7 (8.8)	0.24	104.7 (6.1)	116.6 (8.1)	0.25
CD62L				96.0 (8.5)	122.9 (14.8)	0.14	104.1 (14.7)	125.9 (15.5)	0.32

[a] Mice were infected with 10^2 PFU of WNV in the footpad. Brains were harvested and analyzed by flow cytometry at 7 days after infection. Values indicate the geometric mean fluorescence intensity of the indicated activation or phenotypic marker within CD8^{+}, IFN-γ^{+}, or TNF-α^{+} populations, shown as means (SEMs) of 8 mice per group. Asterisk indicates significant differences between WT and $MDA5^{-/-}$ cells.
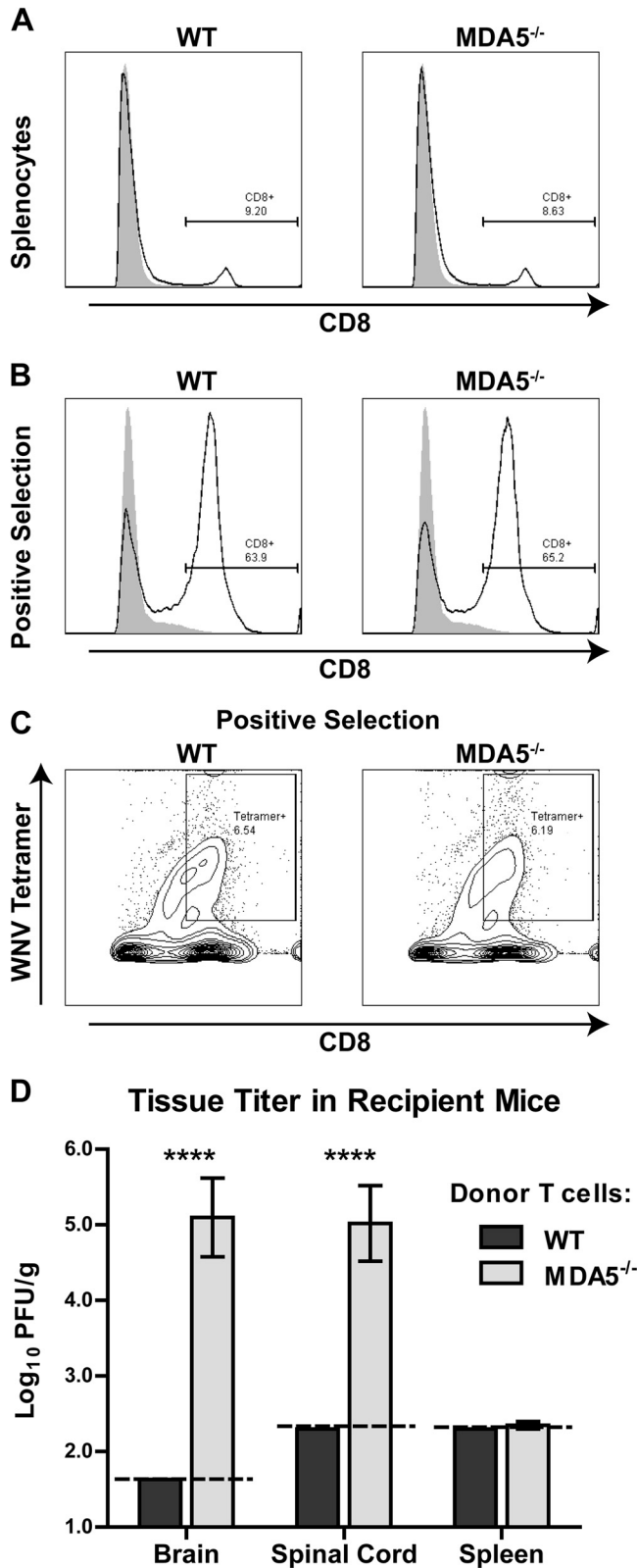
FIG 8 Adoptive transfer of primed donor WT or $MDA5^{-/-}$ CD8$^+$ T cells into recipient infected $CD8^{-/-}$ mice. WT and $MDA5^{-/-}$ mice were infected with 10^2 PFU of WNV in the footpad. At 7 days after infection, CD8$^+$ T cells were purified from splenocytes by positive selection and transferred into $CD8^{-/-}$ mice which had been infected with WNV 1 day prior. (A and B) Flow

the brain and spinal cord. Since WT and $MDA5^{-/-}$ CD8$^+$ T cells were primed equivalently in an $MDA5^{+/+}$ host, we surmise that MDA5 functions in other cell types to optimally activate CD8$^+$ T cells to control WNV infection in the CNS.

Although we observed increased WNV-induced lethality in $MDA5^{-/-}$ mice, this phenotype was less pronounced than that observed in $MAVS^{-/-}$ mice, which lack all RLR signaling; this is most apparent in the mean times to death of the animals (7 days for $MAVS^{-/-}$ versus 11 days for $MDA5^{-/-}$ mice) (31). $MAVS^{-/-}$ mice are less vulnerable to WNV infection than $IRF-3^{-/-} \times IRF-5^{-/-} \times IRF-7^{-/-}$ mice, which are defective at producing type I IFN, or $IFNAR^{-/-}$ mice, which cannot respond to it (77–79). These differences in susceptibility highlight the considerable redundancy present in the pathogen-sensing and downstream signal transduction pathways responsible for initiating the antiviral response. While infections with some viruses, particularly picornaviruses and murine norovirus (22–24) and possibly coronaviruses (25, 26), are sensed largely or exclusively by MDA5, in the context of WNV infection, RIG-I, TLRs, or possibly other PRRs can compensate to some degree for the loss of MDA5 (57, 59–61, 63).

We expected that as a cytoplasmic PRR, MDA5 would act partly in a cell-intrinsic manner to restrict WNV replication, as has been reported after infection with other RNA viruses (24, 27). We failed to observe increased WNV replication in $MDA5^{-/-}$ primary neurons or following direct introduction of the virus into the brain, even though the most prominent viral phenotype after subcutaneous infection was observed in the CNS. This phenotype could reflect functional redundancy with RIG-I in neurons or a lack of expression of MDA5. MDA5 is not expressed in uninfected cortical neurons in culture, and relatively low levels were detected by Western blotting at 24 h after WNV infection compared to levels in myeloid cells (80). Cerebellar granule cell neurons express higher levels of MDA5 following WNV infection than do cortical neurons (81) yet also showed no increase in viral replication in $MDA5^{-/-}$ cells. It remains possible that a cell-intrinsic antiviral effect of MDA5 on WNV occurs in other cell types (e.g., myeloid cell subsets), which could explain the small increase in viremia observed in $MDA5^{-/-}$ mice.

Surprisingly, we observed no defects in type I IFN production in $MDA5^{-/-}$ mice in response to WNV infection. In the study described in our accompanying paper (82), MDA5 has been defined as a PRR sensing "late"-stage viral RNA replication products of WNV infection, whereas RIG-I serves as the primary or early initiator of innate immune signaling. Indeed, mice lacking MDA5 and infected with WNV produced slightly higher levels of type I IFN that correlated with increased viremia, suggesting that the loss of late PRR signaling in the absence of MDA5 supports increased viremia and higher levels of viral PAMPs that trigger increased levels of type I IFN production via alternate PRRs. This outcome contrasts data from other viral infections of $MDA5^{-/-}$ mice: type

cytometry plots showing percentages of CD8$^+$ cells from WT and $MDA5^{-/-}$ splenocytes (A) and following positive selection of CD8$^+$ cells (B). Filled gray plots represent isotype control staining, while open plots represent anti-CD8 staining. (C) Flow cytometry plots showing percentages of WNV antigen-specific CD8$^+$ cells from WT and $MDA5^{-/-}$ mice. (D) Tissues were harvested from $CD8^{-/-}$ mice at 10 days after infection and viral burden was measured by plaque assay. Results represent the means $\pm$ SEMs of 6 mice per group; dotted lines represent the limit of sensitivity of the assay. ****, $P < 0.0001$.
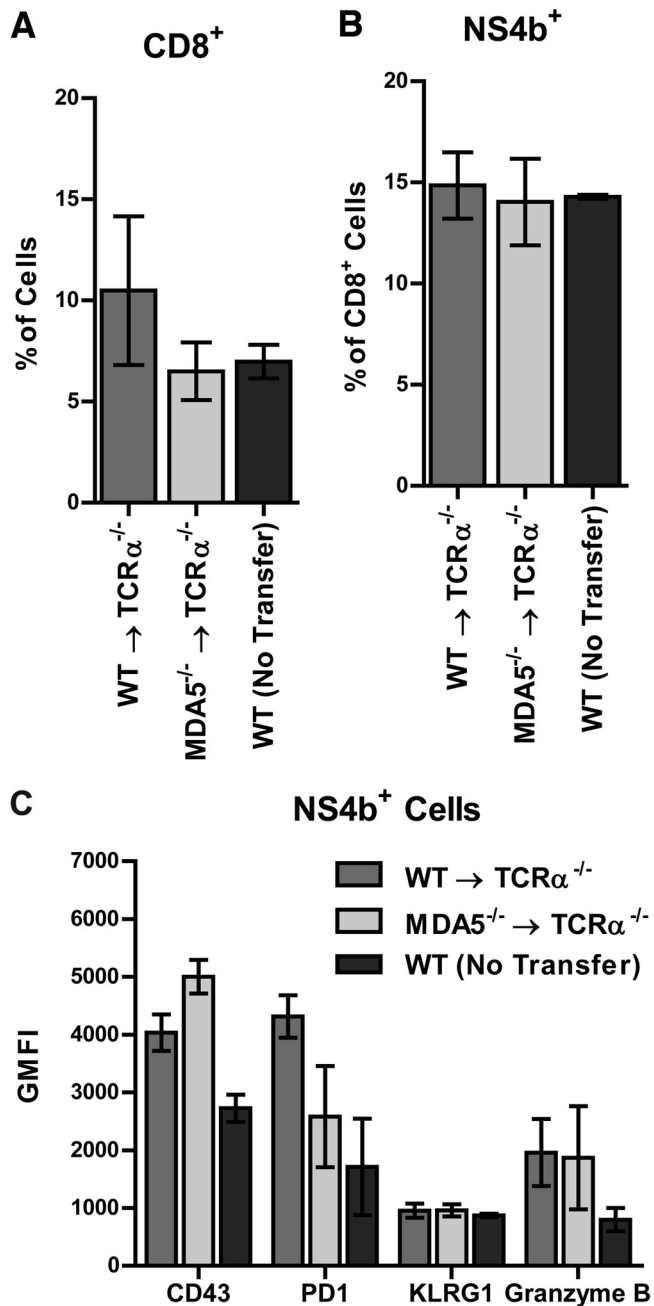
A CD8+

B NS4b+

C NS4b+ Cells

FIG 9 Adoptive transfer of naive donor WT or *MDA5⁻/⁻* CD8⁺ T cells into recipient *TCRα⁻/⁻* mice. CD8⁺ and CD4⁺ T cells were purified by positive selection from naive WT or *MDA5⁻/⁻* splenocytes. WT or *MDA5⁻/⁻* CD8⁺ cells were transferred with WT CD4⁺ cells to *TCRα⁻/⁻* mice. Recipient mice were infected with 10^2 PFU of WNV 1 day following adoptive transfer, and tissues were harvested 9 days after infection. Brains were analyzed by flow cytometry. Percentages of CD8⁺ (A) and WNV antigen-specific (B) infiltrating cells are shown. (C) Expression of CD43, PD1, KLRG1, and granzyme B was measured on NS4B tetramer-positive cells. Results represent the means ± SEMs of 6 mice per group.

I IFN induction was reduced following infection with ECMV, TMEV, CBV, rhinovirus, SeV, HMPV, and LCMV (22, 34, 39–43, 72, 73). In these cases, MDA5 likely serves as a primary PRR of innate immune signaling such that an insufficient type I IFN re-

sponse contributes directly to enhanced viral pathogenesis. Consistent with our results, type I IFN production was sustained in *MDA5⁻/⁻* mice infected with Japanese encephalitis virus, a closely related flavivirus (22). As we observed increased lethality in *MDA5⁻/⁻* mice after WNV infection in the context of sustained type I IFN production and a relatively similar peripheral viral burden, WNV appears to be controlled by a distinct MDA5-dependent pathway.

Although *MDA5⁻/⁻* mice have blunted type I IFN responses to some viral infections, augmented inflammatory responses have been reported, which may contribute to the pathology observed in virus-infected *MDA5⁻/⁻* mice (41, 43). We observed increased accumulation of some inflammatory cytokines and chemokines (i.e., MIP-1β, IL-12, RANTES, and TNF-α) in the brains of *MDA5⁻/⁻* mice, consistent with the increased CNS inflammation observed in *MAVS⁻/⁻* mice following WNV infection (31). The effects of these cytokines on WNV infection and pathogenesis in the CNS are not clear. Clearance of WNV from the CNS requires the recruitment of CD8⁺ T cells (53) and their effector cytokines and functions (74, 83–86), so an increase of inflammatory cytokines may reflect an appropriate immune response to greater viral replication in the CNS of *MDA5⁻/⁻* mice, rather than immunopathology. Indeed, the numbers and proportions of antigen-specific and nonspecific immune cells in the brains of *MDA5⁻/⁻* mice were largely unchanged compared to those in WT animals, even in the context of increased viral load in the CNS, arguing against a dysregulated inflammatory response. While an increase in inflammatory cytokines was seen in *MDA5⁻/⁻* mice after WNV, TMEV, and HMPV infection, reduced levels of several proinflammatory cytokines were observed after infection with rhinovirus and SeV (40–43). This variable role for MDA5 in inflammatory cytokine induction in response to different viral infections may reflect the specific PRR interactions or cellular tropism of each virus.

While the numbers and percentages of infiltrating immune cells in the CNS of WNV-infected *MDA5⁻/⁻* mice were similar to those in WT mice, *MDA5⁻/⁻* CD8⁺ T cells showed increased expression of the exhaustion marker PD-1, which also was observed in *MDA5⁻/⁻* mice infected with TMEV (43). The relationship between PD-1 expression and the function of CNS CD8⁺ T cells in the absence of differences in intracellular cytokine (IFN-γ or TNF-α) expression remains unclear. This phenotype, however, correlated with an intrinsic defect of primed *MDA5⁻/⁻* CD8⁺ T cells to control WNV infection in the CNS of recipient *MDA5⁺/⁺* CD8⁻/⁻ mice. When naive *MDA5⁻/⁻* CD8⁺ T cells were primed in an *MDA5⁺/⁺* environment, no phenotypic differences were observed, suggesting that MDA5 likely is required during the priming process to shape CD8⁺ T cells to function effectively in the CNS. In comparison, in other viral infection models, a deficiency of MDA5 had distinct effects on the CD8⁺ T cell compartment. *MDA5⁻/⁻* mice had fewer antigen-specific CD8⁺ T cells following LCMV infection, although these cells were functional both *ex vivo* and following adoptive transfer to WT mice (73). The quantitative CD8⁺ T cell defects observed in LCMV-infected *MDA5⁻/⁻* mice could be reversed by administration of exogenous type I IFN, suggesting that they occurred secondary to blunted IFN production and are thus unlikely to apply in the context of sustained IFN production that we observed during WNV infection. A T cell-extrinsic role for MDA5 is supported by another study in which MDA5 expression in nonhematopoietic cells en-

hanced survival of antigen-specific $CD8^+$ effector T cells and development into memory cells (75).

MDA5 is not the only RLR that regulates $CD8^+$ T cell function. $CD8^+$ T cell dysfunction in $LGP2^{-/-}$ mice also contributed to WNV pathogenesis, and this was associated with effects on $CD8^+$ T cell death receptor-induced apoptosis through an uncharacterized signaling pathway that was independent of MAVS (38). As LGP2 physically interacts with MDA5 (6, 7), it is conceivable that the observed $CD8^+$ T cell phenotypes in $MDA5^{-/-}$ mice result from MAVS-independent interactions with unbound LGP2, rather than through the canonical RLR signaling pathway. Future studies with $MDA5^{-/-} \times LGP2^{-/-}$ mice and animals with cell type-restricted deletion of MDA5 are planned to address the specific mechanism by which MDA5 regulates $CD8^+$ T cell function against WNV and other viruses.

ACKNOWLEDGMENTS

REFERENCES

1. Wilkins C, Gale M, Jr. 2010. Recognition of viruses by cytoplasmic sensors. Curr. Opin. Immunol. 22:41–47.
2. Rathinam VA, Fitzgerald KA. 2011. Cytosolic surveillance and antiviral immunity. Curr. Opin. Virol. 1:455–462.
3. Takeuchi O, Akira S. 2008. MDA5/RIG-I and virus recognition. Curr. Opin. Immunol. 20:17–22.
4. Takeuchi O, Akira S. 2010. Pattern recognition receptors and inflammation. Cell 140:805–820.
5. Sarkar D, Desalle R, Fisher PB. 2008. Evolution of MDA-5/RIG-I-dependent innate immunity: independent evolution by domain grafting. Proc. Natl. Acad. Sci. U. S. A. 105:17040–17045.
6. Saito T, Hirai R, Loo YM, Owen D, Johnson CL, Sinha SC, Akira S, Fujita T, Gale M, Jr. 2007. Regulation of innate antiviral defenses through a shared repressor domain in RIG-I and LGP2. Proc. Natl. Acad. Sci. U. S. A. 104:582–587.
7. Komuro A, Horvath CM. 2006. RNA- and virus-independent inhibition of antiviral signaling by RNA helicase LGP2. J. Virol. 80:12332–12342.
8. Satoh T, Kato H, Kumagai Y, Yoneyama M, Sato S, Matsushita K, Tsujimura T, Fujita T, Akira S, Takeuchi O. 2010. LGP2 is a positive regulator of RIG-I- and MDA5-mediated antiviral responses. Proc. Natl. Acad. Sci. U. S. A. 107:1512–1517.
9. Venkataraman T, Valdes M, Elsby R, Kakuta S, Caceres G, Saijo S, Iwakura Y, Barber GN. 2007. Loss of DExD/H box RNA helicase LGP2 manifests disparate antiviral responses. J. Immunol. 178:6444–6455.
10. Rothenfusser S, Goutagny N, DiPerna G, Gong M, Monks BG, Schoenemeyer A, Yamamoto M, Akira S, Fitzgerald KA. 2005. The RNA helicase Lgp2 inhibits TLR-independent sensing of viral replication by retinoic acid-inducible gene-I. J. Immunol. 175:5260–5268.
11. Rehwinkel J, Tan CP, Goubau D, Schulz O, Pichlmair A, Bier K, Robb N, Vreede F, Barclay W, Fodor E, Reis e Sousa C. 2010. RIG-I detects viral genomic RNA during negative-strand RNA virus infection. Cell 140:397–408.
12. Pichlmair A, Schulz O, Tan CP, Naslund TI, Liljestrom P, Weber F, Reis e Sousa C. 2006. RIG-I-mediated antiviral responses to single-stranded RNA bearing 5′-phosphates. Science 314:997–1001.
13. Kato H, Takeuchi O, Mikamo-Satoh E, Hirai R, Kawai T, Matsushita K, Hiiragi A, Dermody TS, Fujita T, Akira S. 2008. Length-dependent recognition of double-stranded ribonucleic acids by retinoic acid-inducible gene-I and melanoma differentiation-associated gene 5. J. Exp. Med. 205:1601–1610.
14. Baum A, Sachidanandam R, Garcia-Sastre A. 2010. Preference of RIG-I for short viral RNA molecules in infected cells revealed by next-generation sequencing. Proc. Natl. Acad. Sci. U. S. A. 107:16303–16308.
15. Hornung V, Ellegast J, Kim S, Brzozka K, Jung A, Kato H, Poeck H, Akira S, Conzelmann KK, Schlee M, Endres S, Hartmann G. 2006. 5′-Triphosphate RNA is the ligand for RIG-I. Science 314:994–997.
16. Saito T, Owen DM, Jiang F, Marcotrigiano J, Gale M, Jr. 2008. Innate immunity induced by composition-dependent RIG-I recognition of hepatitis C virus RNA. Nature 454:523–527.
17. Schnell G, Loo YM, Marcotrigiano J, Gale M, Jr. 2012. Uridine composition of the poly-U/UC tract of HCV RNA defines non-self recognition by RIG-I. PLoS Pathog. 8:e1002839. doi:10.1371/journal.ppat.1002839.
18. Wu B, Peisley A, Richards C, Yao H, Zeng X, Lin C, Chu F, Walz T, Hur S. 2013. Structural basis for dsRNA recognition, filament formation, and antiviral signal activation by MDA5. Cell 152:276–289.
19. Childs KS, Andrejeva J, Randall RE, Goodbourn S. 2009. Mechanism of mda-5 inhibition by paramyxovirus V proteins. J. Virol. 83:1465–1473.
20. Yoneyama M, Fujita T. 2007. Function of RIG-I-like receptors in antiviral innate immunity. J. Biol. Chem. 282:15315–15318.
21. Liu HM, Loo YM, Horner SM, Zornetzer GA, Katze MG, Gale M, Jr. 2012. The mitochondrial targeting chaperone 14-3-3epsilon regulates a RIG-I translocon that mediates membrane association and innate antiviral immunity. Cell Host Microbe 11:528–537.
22. Kato H, Takeuchi O, Sato S, Yoneyama M, Yamamoto M, Matsui K, Uematsu S, Jung A, Kawai T, Ishii KJ, Yamaguchi O, Otsu K, Tsujimura T, Koh CS, Reis e Sousa C, Matsuura Y, Fujita T, Akira S. 2006. Differential roles of MDA5 and RIG-I helicases in the recognition of RNA viruses. Nature 441:101–105.
23. Gitlin L, Barchet W, Gilfillan S, Cella M, Beutler B, Flavell RA, Diamond MS, Colonna M. 2006. Essential role of mda-5 in type I IFN responses to polyriboinosinic:polyribocytidylic acid and encephalomyocarditis picornavirus. Proc. Natl. Acad. Sci. U. S. A. 103:8459–8464.
24. McCartney SA, Thackray LB, Gitlin L, Gilfillan S, Virgin HW, Colonna M. 2008. MDA-5 recognition of a murine norovirus. PLoS Pathog. 4:e1000108. doi:10.1371/journal.ppat.1000108.
25. Roth-Cross JK, Bender SJ, Weiss SR. 2008. Murine coronavirus mouse hepatitis virus is recognized by MDA5 and induces type I interferon in brain macrophages/microglia. J. Virol. 82:9829–9838.
26. Züst R, Cervantes-Barragan L, Habjan M, Maier R, Neuman BW, Ziebuhr J, Szretter KJ, Baker SC, Barchet W, Diamond MS, Siddell SG, Ludewig B, Thiel V. 2011. Ribose 2′-O-methylation provides a molecular signature for the distinction of self and non-self mRNA dependent on the RNA sensor Mda5. Nat. Immunol. 12:137–143.
27. Schoggins JW, Wilson SJ, Panis M, Murphy MY, Jones CT, Bieniasz P, Rice CM. 2011. A diverse range of gene products are effectors of the type I interferon antiviral response. Nature 472:481–485.
28. Loo YM, Fornek J, Crochet N, Bajwa G, Perwitasari O, Martinez-Sobrido L, Akira S, Gill MA, Garcia-Sastre A, Katze MG, Gale M, Jr. 2008. Distinct RIG-I and MDA5 signaling by RNA viruses in innate immunity. J. Virol. 82:335–345.
29. Fredericksen BL, Keller BC, Fornek J, Katze MG, Gale M, Jr. 2008. Establishment and maintenance of the innate antiviral response to West Nile virus involves both RIG-I and MDA5 signaling through IPS-1. J. Virol. 82:609–616.
30. Malathi K, Dong B, Gale M, Jr, Silverman RH. 2007. Small self-RNA generated by RNase L amplifies antiviral innate immunity. Nature 448:816–819.
31. Suthar MS, Ma DY, Thomas S, Lund JM, Zhang N, Daffis S, Rudensky AY, Bevan MJ, Clark EA, Kaja MK, Diamond MS, Gale M, Jr. 2010. IPS-1 is essential for the control of West Nile virus infection and immunity. PLoS Pathog. 6:e1000757. doi:10.1371/journal.ppat.1000757.
32. Faul EJ, Wanjalla CN, Suthar MS, Gale M, Wirblich C, Schnell MJ. 2010. Rabies virus infection induces type I interferon production in an IPS-1 dependent manner while dendritic cell activation relies on IFNAR signaling. PLoS Pathog. 6:e1001016. doi:10.1371/journal.ppat.1001016.
33. Wollish AC, Ferris MT, Blevins LK, Loo YM, Gale M, Jr, Heise MT. 2013. An attenuating mutation in a neurovirulent Sindbis virus strain interacts with the IPS-1 signaling pathway in vivo. Virology 435:269–280.
34. Wang JP, Cerny A, Asher DR, Kurt-Jones EA, Bronson RT, Finberg RW. 2010. MDA5 and MAVS mediate type I interferon responses to coxsackie B virus. J. Virol. 84:254–260.

35. Schilte C, Couderc T, Chretien F, Sourisseau M, Gangneux N, Guivel-Benhassine F, Kraxner A, Tschopp J, Higgs S, Michault A, Arenzana-Seisdedos F, Colonna M, Peduto L, Schwartz O, Lecuit M, Albert ML. 2010. Type I IFN controls Chikungunya virus via its action on nonhematopoietic cells. J. Exp. Med. 207:429–442.

36. Rudd PA, Wilson J, Gardner J, Larcher T, Babarit C, Le TT, Anraku I, Kumagai Y, Loo YM, Gale M, Jr, Akira S, Khromykh AA, Suhrbier A. 2012. Interferon response factors 3 and 7 protect against Chikungunya virus hemorrhagic fever and shock. J. Virol. 86:9888–9898.

37. Kato H, Sato S, Yoneyama M, Yamamoto M, Uematsu S, Matsui K, Tsujimura T, Takeda K, Fujita T, Takeuchi O, Akira S. 2005. Cell type-specific involvement of RIG-I in antiviral response. Immunity 23:19–28.

38. Suthar MS, Ramos HJ, Brassil MM, Netland J, Chappell CP, Blahnik G, McMillan A, Diamond MS, Clark EA, Bevan MJ, Gale M, Jr. 2012. The RIG-I-like receptor LGP2 controls CD8(+) T cell survival and fitness. Immunity 37:235–248.

39. McCartney SA, Vermi W, Lonardi S, Rossini C, Otero K, Calderon B, Gilfillan S, Diamond MS, Unanue ER, Colonna M. 2011. RNA sensor-induced type I IFN prevents diabetes caused by a beta cell-tropic virus in mice. J. Clin. Invest. 121:1497–1507.

40. Gitlin L, Benoit L, Song C, Cella M, Gilfillan S, Holtzman MJ, Colonna M. 2010. Melanoma differentiation-associated gene 5 (MDA5) is involved in the innate immune response to Paramyxoviridae infection in vivo. PLoS Pathog. 6:e1000734. doi:10.1371/journal.ppat.1000734.

41. Baños-Lara Mdel R, Ghosh A, Guerrero-Plata A. 2013. Critical role of MDA5 in the interferon response induced by human metapneumovirus infection in dendritic cells and in vivo. J. Virol. 87:1242–1251.

42. Wang Q, Miller DJ, Bowman ER, Nagarkar DR, Schneider D, Zhao Y, Linn MJ, Goldsmith AM, Bentley JK, Sajjan US, Hershenson MB. 2011. MDA5 and TLR3 initiate pro-inflammatory signaling pathways leading to rhinovirus-induced airways inflammation and hyperresponsiveness. PLoS Pathog. 7:e1002070. doi:10.1371/journal.ppat.1002070.

43. Jin YH, Kim SJ, So EY, Meng L, Colonna M, Kim BS. 2012. Melanoma differentiation-associated gene 5 is critical for protection against Theiler's virus-induced demyelinating disease. J. Virol. 86:1531–1543.

44. van der Meulen KM, Pensaert MB, Nauwynck HJ. 2005. West Nile virus in the vertebrate world. Arch. Virol. 150:637–657.

45. Hayes EB, Komar N, Nasci RS, Montgomery SP, O'Leary DR, Campbell GL. 2005. Epidemiology and transmission dynamics of West Nile virus disease. Emerg. Infect. Dis. 11:1167–1173.

46. Johnston LJ, Halliday GM, King NJ. 2000. Langerhans cells migrate to local lymph nodes following cutaneous infection with an arbovirus. J. Invest.Dermatol. 114:560–568.

47. Lim PY, Behr MJ, Chadwick CM, Shi PY, Bernard KA. 2011. Keratinocytes are cell targets of West Nile virus in vivo. J. Virol. 85:5197–5201.

48. Cho H, Diamond MS. 2012. Immune responses to West Nile virus infection in the central nervous system. Viruses 4:3812–3830.

49. Diamond MS, Klein RS. 2004. West Nile virus: crossing the blood-brain barrier. Nat. Med. 10:1294–1295.

50. Sejvar JJ, Haddad MB, Tierney BC, Campbell GL, Marfin AA, Van Gerpen JA, Fleischauer A, Leis AA, Stokic DS, Petersen LR. 2003. Neurologic manifestations and outcome of West Nile virus infection. JAMA 290:511–515.

51. Sejvar JJ. 2007. The long-term outcomes of human West Nile virus infection. Clin. Infect. Dis. 44:1617–1624.

52. Diamond MS, Shrestha B, Marri A, Mahan D, Engle M. 2003. B cells and antibody play critical roles in the immediate defense of disseminated infection by West Nile encephalitis virus. J. Virol. 77:2578–2586.

53. Shrestha B, Diamond MS. 2004. Role of CD8+ T cells in control of West Nile virus infection. J. Virol. 78:8312–8321.

54. Samuel MA, Diamond MS. 2005. Alpha/beta interferon protects against lethal West Nile virus infection by restricting cellular tropism and enhancing neuronal survival. J. Virol. 79:13350–13361.

55. Samuel MA, Diamond MS. 2006. Pathogenesis of West Nile virus infection: a balance between virulence, innate and adaptive immunity, and viral evasion. J. Virol. 80:9349–9360.

56. Suthar MS, Diamond MS, Gale M, Jr. 2013. West Nile virus infection and immunity. Nat. Rev. Microbiol. 11:115–128.

57. Daffis S, Samuel MA, Suthar MS, Gale M, Jr, Diamond MS. 2008. Toll-like receptor 3 has a protective role against West Nile virus infection. J. Virol. 82:10349–10358.

58. Daffis S, Suthar MS, Szretter KJ, Gale M, Jr, Diamond MS. 2009. Induction of IFN-beta and the innate antiviral response in myeloid cells occurs through an IPS-1-dependent signal that does not require IRF-3 and IRF-7. PLoS Pathog. 5:e1000607. doi:10.1371/journal.ppat.1000607.

59. Szretter KJ, Daffis S, Patel J, Suthar MS, Klein RS, Gale M, Jr, Diamond MS. 2010. The innate immune adaptor molecule MyD88 restricts West Nile virus replication and spread in neurons of the central nervous system. J. Virol. 84:12125–12138.

60. Town T, Bai F, Wang T, Kaplan AT, Qian F, Montgomery RR, Anderson JF, Flavell RA, Fikrig E. 2009. Toll-like receptor 7 mitigates lethal West Nile encephalitis via interleukin 23-dependent immune cell infiltration and homing. Immunity 30:242–253.

61. Wang T, Town T, Alexopoulou L, Anderson JF, Fikrig E, Flavell RA. 2004. Toll-like receptor 3 mediates West Nile virus entry into the brain causing lethal encephalitis. Nat. Med. 10:1366–1373.

62. Ebel GD, Dupuis AP, II, Ngo K, Nicholas D, Kauffman E, Jones SA, Young D, Maffei J, Shi PY, Bernard K, Kramer LD. 2001. Partial genetic characterization of West Nile virus strains, New York State, 2000. Emerg. Infect. Dis. 7:650–653.

63. Samuel MA, Whitby K, Keller BC, Marri A, Barchet W, Williams BR, Silverman RH, Gale M, Jr, Diamond MS. 2006. PKR and RNase L contribute to protection against lethal West Nile virus infection by controlling early viral spread in the periphery and replication in neurons. J. Virol. 80:7009–7019.

64. Klein RS, Lin E, Zhang B, Luster AD, Tollett J, Samuel MA, Engle M, Diamond MS. 2005. Neuronal CXCL10 directs CD8+ T cell recruitment and control of West Nile virus encephalitis. J. Virol. 79:11457–11466.

65. Samuel MA, Morrey JD, Diamond MS. 2007. Caspase-3 dependent cell death of neurons contributes to the pathogenesis of West Nile virus encephalitis. J. Virol. 81:2614–2623.

66. Klein RS, Rubin JB, Gibson HD, DeHaan EN, Alvarez-Hernandez X, Segal RA, Luster AD. 2001. SDF-1 alpha induces chemotaxis and enhances Sonic hedgehog-induced proliferation of cerebellar granule cells. Development 128:1971–1981.

67. Thackray LB, Duan E, Lazear HM, Kambal A, Schreiber RD, Diamond MS, Virgin HW. 2012. Critical role for interferon regulatory factor 3 (IRF-3) and IRF-7 in type I interferon-mediated control of murine norovirus replication. J. Virol. 86:13515–13523.

68. Sheehan KC, Lai KS, Dunn GP, Bruce AT, Diamond MS, Heutel JD, Dungo-Arthur C, Carrero JA, White JM, Hertzog PJ, Schreiber RD. 2006. Blocking monoclonal antibodies specific for mouse IFN-alpha/beta receptor subunit 1 (IFNAR-1) from mice immunized by in vivo hydrodynamic transfection. J. Interferon Cytokine Res. 26:804–819.

69. Mehlhop E, Diamond MS. 2006. Protective immune responses against West Nile virus are primed by distinct complement activation pathways. J. Exp. Med. 203:1371–1381.

70. Purtha WE, Myers N, Mitaksov V, Sitati E, Connolly J, Fremont DH, Hansen TH, Diamond MS. 2007. Antigen-specific cytotoxic T lymphocytes protect against lethal West Nile virus encephalitis. Eur. J. Immunol. 37:1845–1854.

71. Brien JD, Uhrlaub JL, Nikolich-Zugich J. 2007. Protective capacity and epitope specificity of CD8(+) T cells responding to lethal West Nile virus infection. Eur. J. Immunol. 37:1855–1863.

72. Zhou S, Cerny AM, Zacharia A, Fitzgerald KA, Kurt-Jones EA, Finberg RW. 2010. Induction and inhibition of type I interferon responses by distinct components of lymphocytic choriomeningitis virus. J. Virol. 84:9452–9462.

73. Wang Y, Swiecki M, Cella M, Alber G, Schreiber RD, Gilfillan S, Colonna M. 2012. Timing and magnitude of type I interferon responses by distinct sensors impact CD8 T cell exhaustion and chronic viral infection. Cell Host Microbe 11:631–642.

74. Shrestha B, Samuel MA, Diamond MS. 2006. CD8+ T cells require perforin to clear West Nile virus from infected neurons. J. Virol. 80:119–129.

75. Wang Y, Cella M, Gilfillan S, Colonna M. 2010. Cutting edge: polyinosinic:polycytidylic acid boosts the generation of memory CD8 T cells through melanoma differentiation-associated protein 5 expressed in stromal cells. J. Immunol. 184:2751–2755.

76. Sitati EM, Diamond MS. 2006. CD4+ T-cell responses are required for clearance of West Nile virus from the central nervous system. J. Virol. 80:12060–12069.

77. Daffis S, Lazear HM, Liu WJ, Audsley M, Engle M, Khromykh AA, Diamond MS. 2011. The naturally attenuated Kunjin strain of West Nile virus shows enhanced sensitivity to the host type I interferon response. J. Virol. 85:5664–5668.

78. Lazear HM, Lancaster A, Wilkins C, Suthar MS, Huang A, Vick SC,

Clepper L, Thackray L, Brassil MM, Virgin HW, Nikolich-Zugich J, Moses AV, Gale M, Jr, Fruh K, Diamond MS. 2013. IRF-3, IRF-5, and IRF-7 coordinately regulate the type I IFN response in myeloid dendritic cells downstream of MAVS signaling. PLoS Pathog. **9**:e1003118. doi:10 .1371/journal.ppat.1003118.

79. Lazear HM, Pinto AK, Vogt MR, Gale M, Jr, Diamond MS. 2011. Beta interferon controls West Nile virus infection and pathogenesis in mice. J. Virol. **85**:7186–7194.

80. Daffis S, Samuel MA, Keller BC, Gale M, Jr, Diamond MS. 2007. Cell-specific IRF-3 responses protect against West Nile virus infection by interferon-dependent and -independent mechanisms. PLoS Pathog. **3**:e106. doi:10.1371/journal.ppat.0030106.

81. Cho H, Proll SC, Szretter KJ, Katze MG, Gale M, Jr, Diamond MS. 2013. Differential innate immune response programs in neuronal subtypes determine susceptibility to infection in the brain by positive-stranded RNA viruses. Nat. Med. **19**:458–464.

82. Errett JS, Suthar MS, McMillan A, Diamond MS, Gale M, Jr. 2013. The essential, nonredundant roles of RIG-I and MDA5 in detecting and controlling West Nile virus infection. J. Virol. **87**:11416–11425.

83. Shrestha B, Diamond MS. 2007. Fas ligand interactions contribute to CD8+ T-cell-mediated control of West Nile virus infection in the central nervous system. J. Virol. **81**:11749–11757.

84. Shrestha B, Pinto AK, Green S, Bosch I, Diamond MS. 2012. CD8+ T cells use TRAIL to restrict West Nile virus pathogenesis by controlling infection in neurons. J. Virol. **86**:8937–8948.

85. Shrestha B, Wang T, Samuel MA, Whitby K, Craft J, Fikrig E, Diamond MS. 2006. Gamma interferon plays a crucial early antiviral role in protection against West Nile virus infection. J. Virol. **80**:5338–5348.

86. Shrestha B, Zhang B, Purtha WE, Klein RS, Diamond MS. 2008. Tumor necrosis factor alpha protects against lethal West Nile virus infection by promoting trafficking of mononuclear leukocytes into the central nervous system. J. Virol. **82**:8956–8964.